The Astrophysical Journal, 722:452–459, 2010 October 10 doi:10.1088/0004-637X/722/1/452

BAYESIAN ANALYSIS OF AN ANISOTROPIC UNIVERSE MODEL: SYSTEMATICS AND POLARIZATION

Nicolaas E. Groeneboom[1,2], Lotty Ackerman[3,4], Ingunn Kathrine Wehus[3,5], and Hans Kristian Eriksen[1,2]
[1] Institute of Theoretical Astrophysics, University of Oslo, P.O. Box 1029 Blindern, N-0315 Oslo, Norway; nicolaag@astro.uio.no, h.k.k.eriksen@astro.uio.no
[2] Centre of Mathematics for Applications, University of Oslo, P.O. Box 1053 Blindern, N-0316 Oslo, Norway
[3] California Institute of Technology, 1200 E. California Blvd., Pasadena, CA 91125, USA; lotty@theory.caltech.edu
[4] Texas Cosmology Center, The University of Texas at Austin, TX 78712, USA
[5] Department of Physics, University of Oslo, P.O. Box 1048 Blindern, N-0316 Oslo, Norway; i.k.wehus@fys.uio.no
Received 2009 November 6; accepted 2010 August 13; published 2010 September 21

ABSTRACT

We revisit the anisotropic universe model previously developed by Ackerman, Carroll, and Wise (ACW), and generalize both the theoretical and computational framework to include polarization and various forms of systematic effects. We apply our new tools to simulated *Wilkinson Microwave Anisotropy Probe* (*WMAP*) data in order to understand the potential impact of asymmetric beams, noise misestimation, and potential zodiacal light emission. We find that neither has any significant impact on the results. We next show that the previously reported ACW signal is also present in the one-year *WMAP* temperature sky map presented by Liu & Li, where data cuts are more aggressive. Finally, we re-analyze the five-year *WMAP* data taking into account a previously neglected $(-i)^{l-l'}$-term in the signal covariance matrix. We still find a strong detection of a preferred direction in the temperature map. Including multipoles up to $\ell = 400$, the anisotropy amplitude for the *W* band is found to be $g = 0.29 \pm 0.031$, nonzero at 9σ. However, the corresponding preferred direction is also shifted very close to the ecliptic poles at $(l, b) = (96, 30)$, in agreement with the analysis of Hanson & Lewis, indicating that the signal is aligned along the plane of the solar system. This strongly suggests that the signal is not of cosmological origin, but most likely is a product of an unknown systematic effect. Determining the nature of the systematic effect is of vital importance, as it might affect other cosmological conclusions from the *WMAP* experiment. Finally, we provide a forecast for the Planck experiment including polarization.

Key words: cosmic background radiation – cosmology: observations – methods: numerical

Online-only material: color figures

1. INTRODUCTION

In recent years, the study of the cosmic microwave background (CMB) has proved to be the most fruitful addition to our understanding of the early universe. Observations of the CMB anisotropies, like those obtained by the *Wilkinson Microwave Anisotropy Probe* (*WMAP*) experiment (Bennett et al. 2003; Hinshaw et al. 2007), have provided us with incomparable insight on the composition of structure in our universe. Combined with previous experimental knowledge and a sound theoretical framework, the concordance model of ΛCDM has been established.

The ΛCDM model relies on the framework of inflation. Inflation was initially proposed as a solution to the horizon and flatness problem (Guth 1981). Additionally, it established a highly successful theory for the formation of primordial density perturbations, providing the required seeds for the large-scale structures (LSS). Eventually, these later gave rise to the temperature anisotropies in the CMB radiation that we observe today (Guth 1981; Linde 1982, 1983, 1994; Mukhanov & Chibisov 1981; Starobinsky 1982; Smoot 1992; Ruhl 2003; Rynyan 2003; Scott et al. 2003).

One of the predictions from inflation is that the observed universe should be nearly isotropic on large scales. However, anomalies found in the CMB during recent years (de Oliveira-Costa et al. 2004; Vielva et al. 2004; Eriksen et al. 2004a) suggest that anisotropic inflationary models should be considered. A specific example is the generalized model presented by Ackerman et al. (2007), which considers violation of rotational invariance in the early universe. A general framework for describing similar models was presented by Pullen & Kamionkowski (2007).

Himmetoglu et al. (2009a, 2009b) showed that the anisotropic inflationary background of the Ackerman, Carroll, and Wise (ACW) model characterized by a fixed-norm vector field ultimately is unstable. However, the parameterization of the signal covariance matrix is independent of that unstable model. It represents general correlations induced by rotations in the CMB at a phenomenological level. Several papers have recently investigated the properties of the ACW model with extensions (Hou et al. 2009; Karčiauskas et al. 2009; Dimopoulos et al. 2009; Carroll et al. 2010; Dvorkin et al. 2008; Valenzuela-Toledo et al. 2009; Valenzuela-Toledo & Rodriguez 2009).

Work in this field suggests that the five-year *WMAP* data contain a significant ACW-anisotropic signal, corresponding to a 3.8σ detection in the *W* band (Groeneboom & Eriksen 2009). A more recent paper by Hanson & Lewis (2009) points out that the direction is incorrect due to a neglected factor of $(-i)^{l-l'}$ corrected in a later version of Ackerman et al. (2007), yielding an ACW signal in which the preferred direction is located very close to the ecliptic poles.

In this paper, we re-analyze the five-year *WMAP* data including the previously neglected $(-i)^{l-l'}$-factor, and investigate whether traces of the ACW-anisotropic contribution signal are still evident. The analysis will, as previously, be performed with the CMB Gibbs sampling framework (Jewell et al. 2004; Wandelt et al. 2004; Eriksen et al. 2004b), which by Groeneboom & Eriksen (2009) was included to allow for non-diagonal, but sparse covariance matrices. This framework allows for exact Bayesian analysis of high-resolution CMB data with

a non-diagonal CMB signal covariance matrix. The isotropic method has already been applied several times to the *WMAP* data (O'Dwyer et al. 2004; Eriksen et al. 2007a, 2007b, 2008a), and has already been extended to take into account polarization (Larson et al. 2007) and internal component separation (Eriksen et al. 2008b).

In our re-analysis of the five-year *WMAP* temperature data, we confirm that the direction is shifted to the ecliptic poles, at a greatly increased significance. As the north and south ecliptic poles are aligned with our solar system, the ACW signal in the *WMAP* data is therefore most likely a systematic effect and not of cosmological origin. This is in complete agreement with Hanson & Lewis (2009).

It has not yet been possible to fully rule out whether any known systematic effect could have contributed to the signal. In theory, either asymmetric beams, misestimated noise or even the zodiacal light could have affected the detection of the ACW signal. We consider these three effects and conclude that all have negligible impacts on the ACW signal.

Until now, the framework has only supported temperature–temperature (TT) correlations. Here, we extend the mechanics to include E-mode correlations (EE), including cross-mode correlations (TE). We then provide a forecast for the upcoming Planck experiment, considering simulated T+E maps. The Planck data will hopefully be able to rule out all doubts about the origin of the ACW signal.

2. RE-ANALYSIS OF FIVE-YEAR TEMPERATURE *WMAP* DATA

Ackerman et al. (2007) and Hanson & Lewis (2009) pointed out an error in the expression for the off-diagonal covariance matrix. The expression for the signal covariance matrix in Equations (4) and (5) now includes a previously neglected factor of $(-i)^{l-l'}$. For the ACW covariance matrix that correlates scales with $\ell = \ell' \pm 2$, the only difference in contribution is $(-i)^{\pm 2} = -1$, negating the off-diagonal terms. Hanson & Lewis (2009) claim that the ACW signal direction in the five-year *WMAP* data is located at the ecliptic poles, and not at $(l, b) = (110^\circ, 30^\circ)$, as presented by Groeneboom & Eriksen (2009). In light of the new results, we perform a new full temperature analysis of the *WMAP* data and investigate whether the neglected factor has any impact on the resulting posteriors.

2.1. Data

We consider the five-year *WMAP* temperature sky maps (Hinshaw et al. 2009) and analyze the *Q*, *V*, and *W* bands (41, 61, and 94 GHz), where the *W* and *V* bands are assumed to be the cleanest *WMAP* bands in terms of residual foregrounds. We adopt the template-corrected, foreground reduced maps recommended by the *WMAP* team for cosmological analysis, and impose the KQ85 masks (Gold et al. 2009), which remove 18% of the sky. Point source cuts are imposed in both masks.

We analyze the data frequency-by-frequency and consider the combinations V1+V2, Q1+Q2, and W1 through W4. The noise rms patterns and beam profiles are taken into account for each difference assembly (DA) map individually. The noise is assumed uncorrelated. All data used in this analysis are available from LAMBDA.[6]

[6] http://lambda.gsfc.nasa.gov/

Table 1
Summary of Marginal Posteriors from WMAP5

Band	ℓ Range	Mask	Amplitude g_*	Direction (l, b)
W1-4	2–400	KQ85	0.29 ± 0.031	$(94^\circ, 26^\circ) \pm 4^\circ$
V1-2	2–400	KQ85	0.14 ± 0.034	$(97^\circ, 27^\circ) \pm 9^\circ$
Q1-2	2–300	KQ85	-0.18 ± 0.040	$(99^\circ, 28^\circ) \pm 10^\circ$

Notes. The values for g_* indicate posterior mean and standard deviation. The ecliptic poles are located at $\pm(96^\circ, 30^\circ)$.

2.2. Results

The results from our analysis are presented in Table 1, and the posteriors are shown in Figure 1. The strongest detection is still present in the *W* band, where $g_* = 0.29 \pm 0.031$, corresponding to a 9σ detection. However, the correction term mentioned above clearly has a significant effect on the signal described by Groeneboom & Eriksen (2009). The direction and the significance of the detection are altered: for both the *W*-band and *V*-band analyses, the preferred direction is now located at $(l, b) = \pm(96^\circ, 30^\circ)$, very close to the north/south ecliptic poles. In addition, the significance of the signal in the *W* band is increased from previously 3.8σ to about 9σ, showing that the neglected correction term has "forced" the signal away from its true direction—the north and south ecliptic poles. The probability that this direction is a pure coincidence is minimal, and the observed signal is therefore most likely a product of systematics. Another interesting fact is that the signal seems to be frequency dependent, with a stronger signal in the *W* bands than in the *V* bands. Further, the *Q* bands seem to exhibit a negative g_*, which suggests frequency dependence. In addition, we analyze the independent *W*-band data sets, and find that the anisotropic amplitude g_* is consistent to about 1σ within the frequency average amplitude.

3. ANALYSIS OF SYSTEMATIC EFFECTS

Before the correction was introduced, we performed several tests on the independent *WMAP* five-year DA bands showing that the direction is both existent and stable in bands. The significance was also slightly increased, and we are able to cover the signal up to $\ell_{\max} = 700$. We now proceed by investigating various systematic effects as candidates for the observed signal. A visualization of some possible sources of systematic effects together with a realization of the ACW signal for comparison is presented in Figure 2: asymmetric beams (upper right), noise rms maps (bottom left), and the zodiacal light template (lower right).

3.1. Impact of Noise Misestimation

One of the possible candidates for generating the ACW signal found by Groeneboom & Eriksen (2009) is noise mischaracterization. Previous work done by Groeneboom & Eriksen (2009) showed that correlated noise levels have little or no effect on the signal. We have re-analyzed the *WMAP* data using the previously neglected $(-i)^{l-l'}$-term, but find no evidence for effects from correlated noise.

However, it might be possible that noise with incorrect rms specifications could give rise to a signal similar as the ACW signal. We therefore perform one more analysis to test noise sensitivity.

Groeneboom et al. (2009) discovered that the noise levels provided by the *WMAP* team were slightly off by about 0.5%–1%.

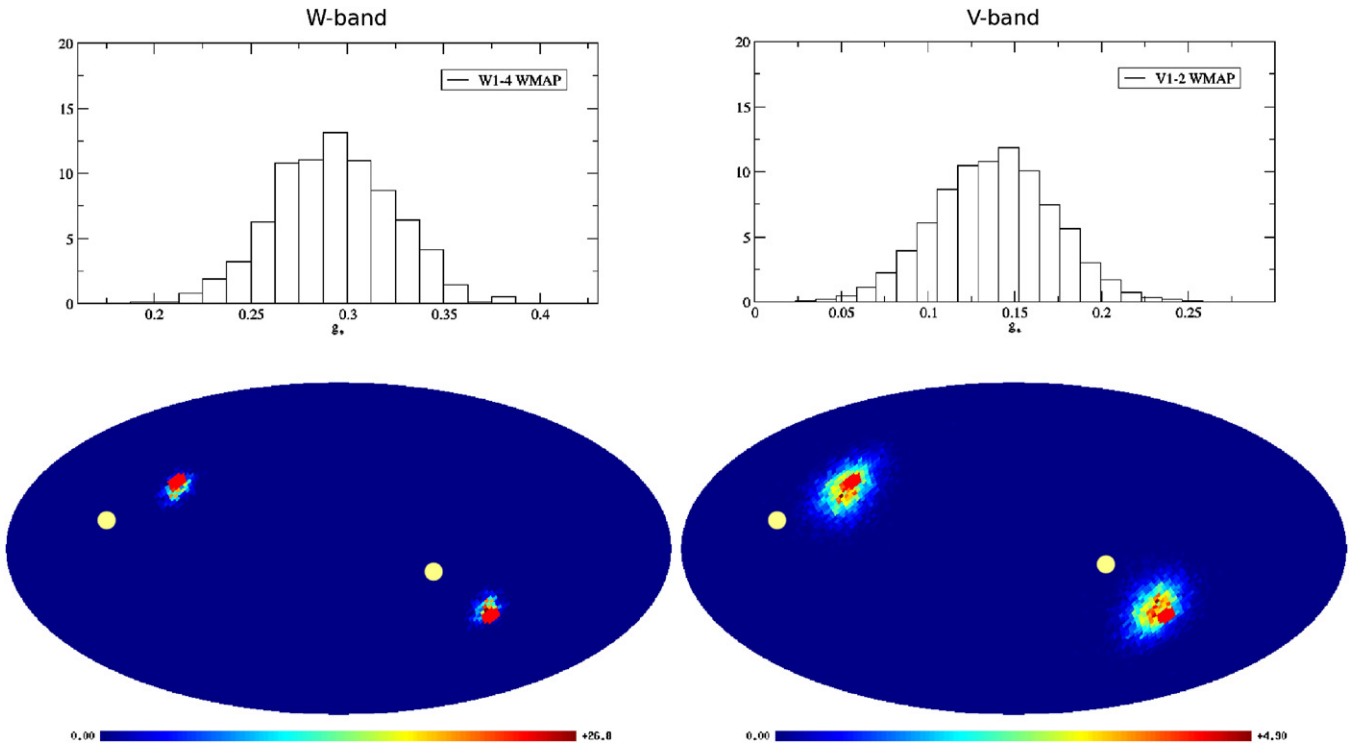

Figure 1. *W*- and *V*-band posteriors for the temperature analysis, using $\ell_{\rm cutoff} = 400$ and the KQ85 mask. The north and south ecliptic poles are marked with a red circle. Note how the posterior peaks correspond with the ecliptic poles. The yellow circles indicate the direction from the previous analysis by Groeneboom & Eriksen (2009).

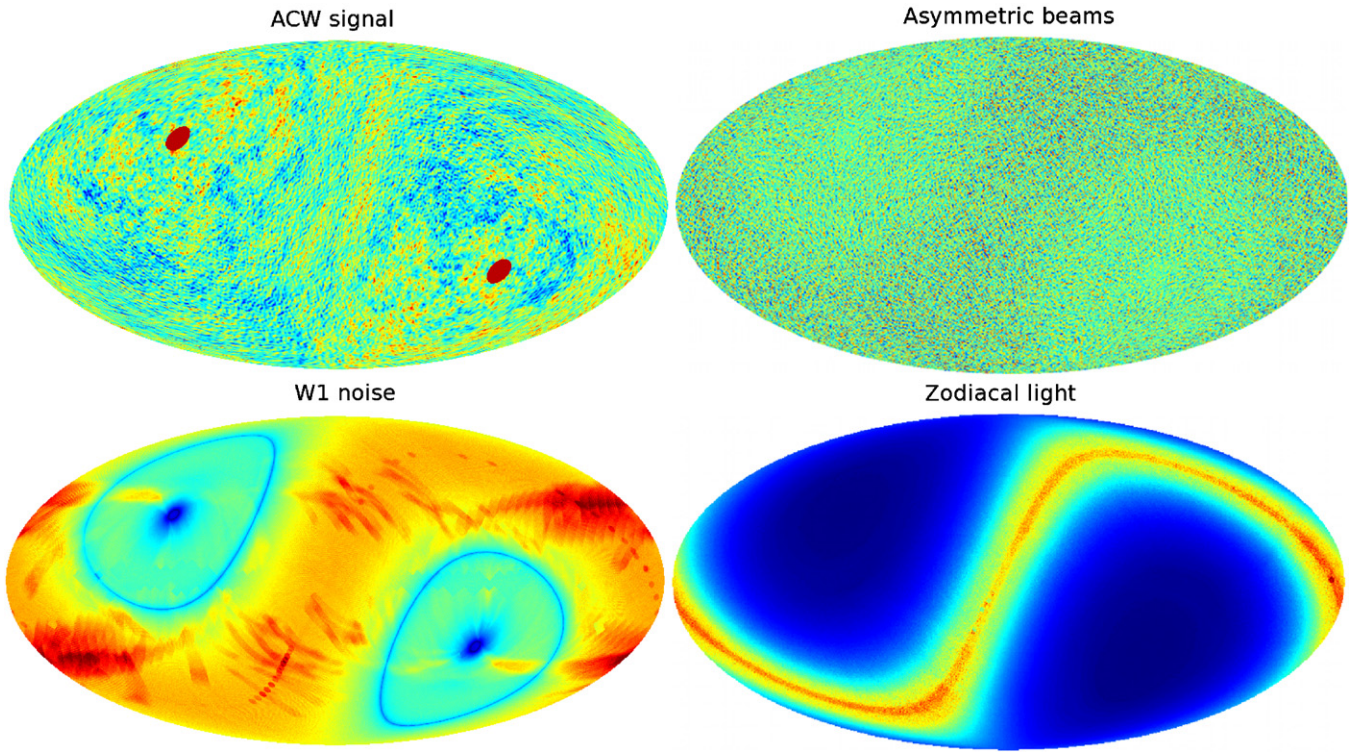

Figure 2. Various systematic effects compared with the ACW signal (upper left). Asymmetric beams (upper right), noise maps (bottom left), and the zodiacal light template (lower right) are similar in shape to the ACW signal, and could therefore be thought to contribute to the ACW signal in the *WMAP* data.

While this error is small enough to not significantly affect most cosmological analyses, it is conceivable that incorrect noise levels could contribute to a signal similar to the ACW model.

We therefore simulate a V1 map with 5% incorrect V1 noise, i.e., the noise is multiplied with 1.05 before it is added to the map. The analysis is done with the $KQ85$ mask. The χ^2

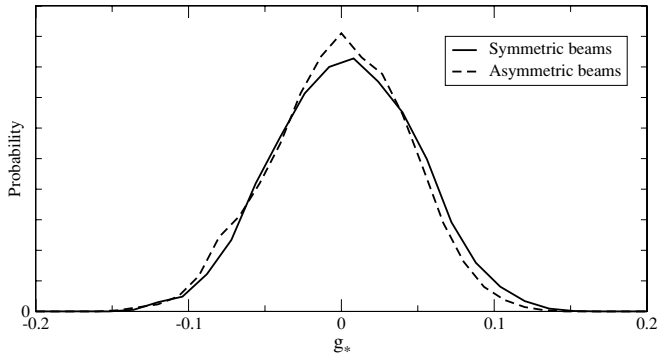

Figure 3. Analysis of the same isotropic map convolved with symmetric (black) and asymmetric (red) beams. Note how both results are consistent with $g_* = 0$.

comes out about 6% above the expected value, recording that the incorrect noise is measured by the Gibbs sampler. However, the posteriors still show a zero detection of the ACW model, with an anisotropic amplitude of $g_* = 0.01 \pm 0.05$. This indicates that incorrect noise levels have little or no effect on the ACW signal.

3.2. Impact of Asymmetric Beams

Another issue with the analysis of Groeneboom & Eriksen (2009) is whether the asymmetric beams of the *WMAP* detectors could have given rise to a signal similar to the ACW model. Wehus et al. (2009) established a full framework for simulating *WMAP* maps with asymmetric beams. An example of contribution from asymmetric beams on *WMAP* maps is presented in Figure 2. The authors also provided a set of 10 simulated maps with asymmetric beams. We now perform a Bayesian analysis on these maps, together with an analysis on isotropic simulated maps with symmetric beams for comparison.

The test data are set up as such: we simulate isotropic test maps with the best-fit ΛCDM power spectrum, and convolve them with the standard symmetric V-beams. We then add *V*-band noise rms to the maps, and analyze the test maps. We used the *V*-band setup due to its reduced foreground contamination and correlated noise when compared to the *W*-band data.

We then perform the same analysis on the *V*-band maps from Wehus et al. (2009), which were produced with asymmetric beams. Both analyses are performed using isotropic scales up to $l_{\rm max} = 700$ and anisotropic scales up to $l_{\rm max}^{\rm cutoff} = 512$, with a standard *V*-band setup using the KQ85 mask.

The posteriors for the anisotropy amplitude g_* are shown in Figure 3, with both having $g_* = -0.01 \pm 0.05$. It should be clear that asymmetric beams do not produce effects in the CMB similar to the ACW model, as the analysis shows no trace of any signal detection.

3.3. Zodiacal Light

In this paper, we have seen that the ACW signal in the *WMAP* data has shifted to the ecliptic poles. This indicates that the signal is most likely not of cosmological origin, as it is strongly aligned in the plane of the solar system. An interesting question is whether the ACW signal is connected to the zodiacal light. Zodiacal light is produced by Sun rays reflecting off dust particles sharing the same orbit as the Earth, and share a similar overall structure as the ACW signal. An illustration of a zodiacal light template is presented in Figure 2, together with the estimated ACW signal in the direction of the ecliptic poles. The zodiacal light template was created by T. Banday based on the DIRBE zodiacal light emission model described by Kelsall et al. (1998). We perform three analyses of realistic *V*-band simulations, where we co-add the zodiacal light template to simulated, isotropic *V*-band simulated maps. In the first run, we add the template as it is, in the second and third analyses we multiply the template with a factor of 10 and 100, respectively. In all of the analyses, the posteriors resulted in zero detections with $g_* = 0.0 \pm 0.045$ and no significant directions on the sky, with uniform distributions. We therefore conclude that the zodiacal light does not have a significant contribution to the ACW signal in the *WMAP* data.

3.4. Analyzing Alternative WMAP Data

Liu & Li (2009a, 2009b) have developed an alternative framework for building one-year *WMAP* maps from raw data. The authors imposed stronger constraints on data selection, removing almost 20% of the time-ordered data. For instance, data for which the beam boresight distance from the planets are less than 7° are removed, corresponding to the antenna main beam radius. The temperature map published by the *WMAP* team used a cut of only 1.°5 (Limon et al. 2008). Liu & Li (2009a) also used an extended KQ85 mask which removes 28.3% of the sky. Liu & Li (2009b) claim that the pixels in the *WMAP* scan ring of a hot pixel are systematically cooled, where the strongest anti-correlations between temperatures of a hot pixel and its scan ring appear at a separation angle of about 141°. Due to the anti-correlation of pixels and the strict data cuts, the temperature power spectrum obtained by Liu & Li (2009a) is decreased on average by about 13%, causing the best-fit cosmological parameters to change considerably.

In order to see whether the anti-correlated pixels in the *WMAP* stream could have contributed to the ACW signal in the *WMAP* data, we perform a full temperature analysis on both the alternative temperature map provided by Liu & Li (2009a) and the original one-year *WMAP* temperature map. The map used in our analysis is the V1 band. The rms noise map for the alternative analysis is provided by Liu & Li (2009a), while the maps for the standard *WMAP* analysis were downloaded from the Lambda site. The V1 beam is the same in both cases, as is the extended KQ85 mask from Liu & Li (2009a). If the ACW signal is detected in the *WMAP* data but not the data from Liu & Li (2009a), it might be an indication that the *WMAP* team have included data that should have been left out, giving rise to a correlation structure similar to that of the ACW signal.

Analyzing the maps up to $\ell_{\rm max} = 400$, we find that both maps do contain a significant anisotropic signal, with $g_* \sim 0.15 \pm 0.10$. This implies that the ACW signal is most likely a more intrinsic part of the *WMAP* data, and not due to the possible anti-correlation of pixels.

4. THE ACW MODEL WITH POLARIZATION

We are interested in the signatures that the ACW model would leave on the polarization of the CMB and focus our attention on the scalar perturbations. This calculation was first performed by Pullen & Kamionkowski (2007). Observing the CMB sky in the direction $\hat{\mathbf{e}}$ provides information on the E-mode polarization constructed from the Stokes parameters $Q(\hat{\mathbf{e}})$ and $U(\hat{\mathbf{e}})$, as well as the temperature $T(\hat{\mathbf{e}})$. One can express the respective maps in terms of the spherical-harmonic coefficients $a_{E,lm}$ and $a_{T,lm}$

which are given for each $X = \{E, T\}$ by

$$a_{X,lm} = \int d\Omega_{\mathbf{e}} Y^*_{lm}(\mathbf{e}) \times \int d\mathbf{k}\, \delta(\mathbf{k}) \left(\frac{2l+1}{4\pi}\right) (-i)^l P_l(\hat{\mathbf{k}}\cdot\mathbf{e}) \Theta^{(S)}_{X,l}(k). \quad (1)$$

Here, $Y_{lm}(\mathbf{e})$ denotes the spherical harmonics, $P_l(\mathbf{k})$ are the Legendre polynomials, and $\Theta^{(S)}_{X,l}(k)$ is the lth moment of the transfer function of scalar modes, for either temperature or polarization. Further, $\delta(\mathbf{k})$ is a random variable that characterizes the initial amplitude of the mode and satisfies

$$\langle \delta(\mathbf{k}) \delta^*(\mathbf{q}) \rangle = P'(\mathbf{k}) \delta^3(\mathbf{k} - \mathbf{q}). \quad (2)$$

The ACW model proposes that if we drop the assumption of statistical isotropy by having a preferred direction $\hat{\mathbf{n}}$ during inflation, the primordial power spectrum at leading order has the form

$$P'(\mathbf{k}) = P(k)(1 + g(k)(\hat{\mathbf{k}}\cdot\hat{\mathbf{n}})^2). \quad (3)$$

Here, $g(k)$ is a general function of k, which ACW argue is well approximated by a constant, g_*.

To study the statistics of the CMB produced by the scalar perturbations, we need the power spectrum of the T-, E-modes and the cross-correlation between them. Using the expressions (1) and (3), we can write the various correlations for $X = \{E, T\}$ as

$$\langle a_{X,lm} a^*_{X',l'm'} \rangle = \delta_{ll'} \delta_{mm'} C^{XX'}_{l,l} + g_* \xi_{lm;l'm'} C^{XX'}_{l,l'}, \quad (4)$$

where the $C^{XX'}_{l,l'}$ are given by

$$C^{XX'}_{l,l'} = (-i)^{l-l'} \int_0^\infty dk k^2 P(k) \Theta^{(S)}_{X,l}(k) \Theta^{(S)}_{X',l'}(k). \quad (5)$$

The coefficients $\xi_{lm;l'm'}$ encode the departure from isotropy and connect l with $l' = \{l, l \pm 2\}$ and m with $m' = \{m, m \pm 1, m \pm 2\}$ (Ackerman et al. 2007). Note that the factor of $(-i)^{l-l'}$ was missing in the first version of the paper.

5. THE POLARIZED ANISOTROPIC CMB GIBBS SAMPLER

CMB data observations can be modeled as

$$\mathbf{d} = \mathbf{A}\mathbf{s} + \mathbf{n}, \quad (6)$$

where $\mathbf{d}$ represents the observed data, $\mathbf{A}$ denotes convolution by an instrumental beam, $\mathbf{s}(\theta, \phi) = \sum_{\ell,m} a_{\ell m} Y_{\ell m}(\theta, \phi)$ is the CMB sky signal represented in either harmonic or real space, and $\mathbf{n}$ is instrumental noise. It is generally a good approximation to assume both the CMB and noise to be zero mean Gaussian distributed variates, with covariance matrices $\mathbf{S}$ and $\mathbf{N}$, respectively. In harmonic space, the signal covariance matrix is defined by $\mathbf{S}_{\ell m,\ell' m'} = \langle a_{\ell m} a^*_{\ell' m'} \rangle$. In the isotropic case, this matrix is diagonal. The connection to cosmological parameters ω is made through this covariance matrix. Finally, for experiments such as *WMAP*, the noise is often assumed uncorrelated between pixels, $\mathbf{N}_{ij} = \sigma_i^2 \delta_{ij}$, for pixels i and j, and noise rms equals to σ_i.

Let ω denote a set of cosmological parameters. Our goal is to compute the full joint posterior $P(\omega|\mathbf{d})$, which is given by $P(\omega|\mathbf{d}) \propto P(\mathbf{d}|\omega)P(\omega) = \mathcal{L}(\omega)P(\omega)$, where $\mathcal{L}(\omega)$ is the likelihood and $P(\omega)$ a prior. For a Gaussian data model, the likelihood is expressed as

$$\mathcal{L}(\omega) \propto \frac{e^{-\frac{1}{2}\mathbf{d}^T \mathbf{C}^{-1}(\omega)\mathbf{d}}}{\sqrt{|\mathbf{C}(\omega)|}}, \quad (7)$$

where $\mathbf{C} = \mathbf{S} + \mathbf{N}$ is the total covariance matrix.

5.1. The Gibbs Sampler

The problem of extracting the cosmological signal $\mathbf{s}$ and ω from the full signal by Gibbs sampling was addressed by Jewell et al. (2004), Wandelt et al. (2004), and Eriksen et al. (2004b). The CMB Gibbs sampler is an exact Monte Carlo Markov chain (MCMC) method that assumes prior knowledge of the conditional distributions in order to gain knowledge of the full joint distribution. A significant fraction of the CMB data is completely dominated by galactic foreground, and about 20% of the data needs to be removed. This might sound trivial, but in reality it complicates processes as the spherical harmonics no longer are orthogonal. The Gibbs sampler solves this problem intrinsically, as the galaxy mask becomes a part of the framework (Groeneboom 2009).

The main motivation for introducing the CMB Gibbs sampler is the drastic improvement in scaling. With conventional MCMC methods, one needs to sample the angular power spectrum, $C_\ell = \langle a_{\ell m} a^*_{\ell m} \rangle$, from the distribution $P(C_\ell|\mathbf{d})$, which scales as $\mathcal{O}(N^3_{\rm pix})$, where $N_{\rm pix}$ is the size of the covariance matrix. For a white noise case, the Gibbs sampler reduces this to $\mathcal{O}(N^{1.5}_{\rm pix})$. In other words, the Gibbs sampler enables effective sampling in the high-ℓ regime.

5.2. Sampling Scheme

In order to sample from the full joint distribution $P(C_\ell, \omega, \mathbf{s}|\mathbf{d})$ using the Gibbs sampler, we must know the exact conditional distributions $P(\mathbf{s}|C_\ell, \omega, \mathbf{d})$ and $P(C_\ell, \omega|\mathbf{s})$. The Gibbs sampler then proceeds by alternating sampling from each of these distributions:

$$(C_\ell, \omega)^{i+1} \leftarrow P(C_\ell, \omega|\mathbf{s}^i, \mathbf{d}), \quad (8)$$

$$\mathbf{s}^{i+1} \leftarrow P(\mathbf{s}|(C_\ell, \omega)^{i+1}, \mathbf{d}). \quad (9)$$

The first conditional distribution is expressed as

$$P(C_\ell, \omega|\mathbf{s}, \mathbf{d}) = \frac{e^{-\frac{1}{2}\mathbf{s}^T \mathbf{S}(\omega)^{-1}\mathbf{s}}}{\sqrt{|\mathbf{S}(\omega)|}}, \quad (10)$$

and is distributed according to an inverse Gamma function with $2\ell - 1$ degrees of freedom. The remaining conditional distribution is

$$P(\mathbf{s}|C_\ell, \omega, d) \propto e^{-\frac{1}{2}(\mathbf{s}-\hat{\mathbf{s}})^T (\mathbf{S}(\omega)^{-1} + \mathbf{N}^{-1})(\mathbf{s}-\hat{\mathbf{s}})}, \quad (11)$$

where $\hat{\mathbf{s}} = \mathbf{N}^{-1}\mathbf{d}$. In other words, $P(\mathbf{s}|C_\ell, \omega, \mathbf{d})$ is a Gaussian distribution with mean $\hat{\mathbf{s}}$ and covariance $(\mathbf{S}(\omega)^{-1} + \mathbf{N}^{-1})^{-1}$. Numerical methods for sampling from these distributions were discussed by Groeneboom (2009), and the details on how the polarization covariance matrix was numerically implemented can be found in the Appendix.

6. FORECASTS FOR PLANCK WITH POLARIZATION

The Planck satellite will provide us with high-resolution CMB data of superior quality compared to previous CMB experiments. The Planck experiment also provides high-resolution

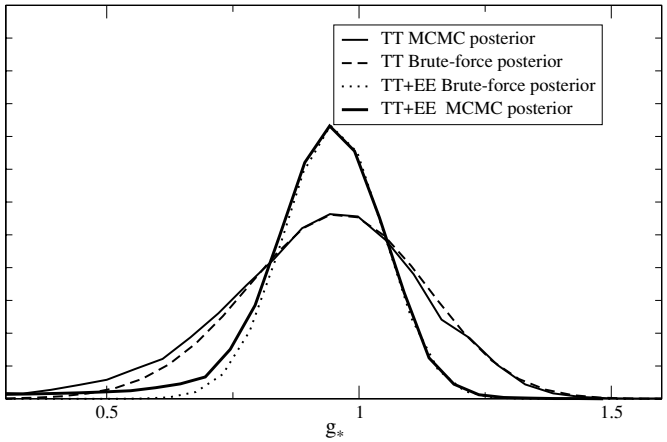

Figure 4. g_* posteriors for several analysis of noiseless simulated $\ell_{\rm max} = 64$ map, using both MCMC and brute-force calculations. Note how the polarization data narrow the distribution.

polarization data, with an ℓ-range up to 2500. As the Planck data are independent from *WMAP* data, it will be very interesting to see whether the ACW signal is evident or not in the data. We therefore need to investigate some anisotropic properties of typical Planck data in order to know what to expect and not expect.

In this section, we set up a high-ℓ temperature analysis with $\ell_{\rm max}^{\rm cutoff} = 800$ and a joint temperature and polarization analysis with $\ell_{\rm max}^{\rm cutoff} = 400$. We then analyze the maps to obtain the posterior means and standard deviation. We continue by forecasting how the standard deviation of the anisotropic amplitude posteriors should vary with multipoles ℓ, as done by Groeneboom & Eriksen (2009).

6.1. Validation of the Polarized Sampler

Before performing a full-scale analysis of simulated polarized Planck data, we wish to validate our code. We therefore simulate a low-resolution $N_{\rm side} = 32$ map with E-mode data included. Assuming an anisotropic amplitude of $g_* = 1.0$, we perform both a brute-force and a metropolis-hastings analysis of a full-sky map with no beam nor noise. The resulting posteriors for the TT-case and the TT+TE+EE-case are shown in Figure 4. It is worth to note that the posterior is more narrow when including polarization data, as there are more data available. A typical

Table 2
Summary of Marginal Posteriors from Simulated Planck Data

Simulated Data	Input Amplitude	ℓ-range	Mask	Estimated g_*
Low-ℓ TT	0.10	2–400	KQ85	0.11 ± 0.025
High-ℓ TT	0.10	2–800	KQ85	0.11 ± 0.020
Low -ℓ TT+TE+EE	0.10	2–400	KQ85	0.10 ± 0.020

Note. The values for g_* indicate the posterior mean and standard deviation.

posterior of the estimated direction n together with the input TT+EE ACW signal is seen in Figure 5.

6.2. Simulations

We now consider a Planck simulation. We first simulate a temperature-only ACW-anisotropic map with $n_{\rm side} = 1024$, $\ell_{\rm max} = 2000$, and $\ell_{\rm cutoff} = 1024$, with a preferred direction pointing toward $(\theta, \phi) = (57^\circ, 57^\circ)$ and an anisotropy amplitude of $g_* = 0.1$, using the best-fit five-year *WMAP* ΛCDM power spectrum (Komatsu et al. 2009). The map is convolved with a Gaussian beam corresponding to the 143 GHz Planck channel, and white, uniform noise is finally added. The beam FWHM for this frequency channel is $7\farcm1$, and the temperature noise rms per $N_{\rm side} = 1024$ pixel is $\sigma_T = 12.2\,\mu$K. The polarization noise rms is $\sigma_P = 23.3\,\mu$K (The Planck Collaboration 2006).

6.3. Results

We perform three analyses of the simulated Planck sky map. The first is an analysis on low-ℓ ($l_{\rm max}^{\rm cutoff} = 400$) temperature data, the second high-ℓ ($l_{\rm max}^{\rm cutoff} = 800$) temperature data while the third is a low-ℓ analysis of TT+TE+EE polarization data. The results are shown in Table 2, where we reproduced the input parameters with typically $g_* = 0.11 \pm 0.025$. Note how the standard deviation of the posterior is lower than for the *WMAP* case. This is to be expected, as higher multipoles ℓ contribute more to the anisotropic effect, but not significantly. This is due to the fact that the off-diagonal correlation terms in the covariance matrix have a lower value on smaller scales.

We determine the standard deviation of the g_* posterior as a function of multipoles ℓ by simulating an unconvolved, noiseless isotropic map including polarization data using the best-fit ΛCDM power spectrum. We then analyze this map for various ℓ, obtaining the posterior distribution for each run. The results are seen in Figure 6. Here, we see that $\sigma(\ell_*)$ is very close

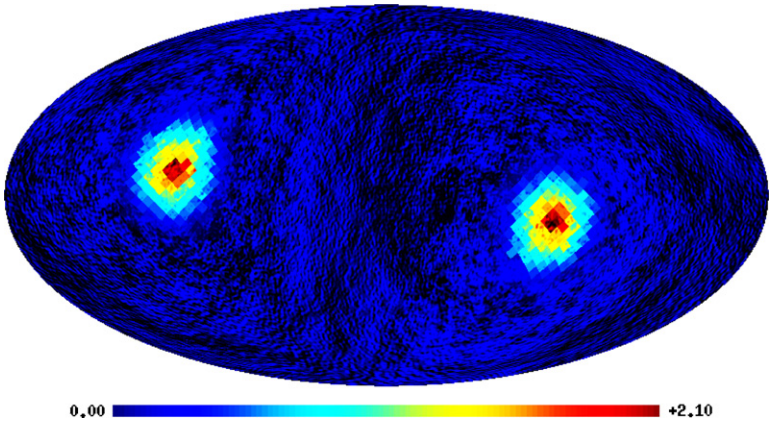

Figure 5. Posterior from a simulated set with $g_* = 1.0$. The original temperature ACW signal in the input map can be seen in the background. Note how the estimated direction corresponds well with the posterior.
(A color version of this figure is available in the online journal.)

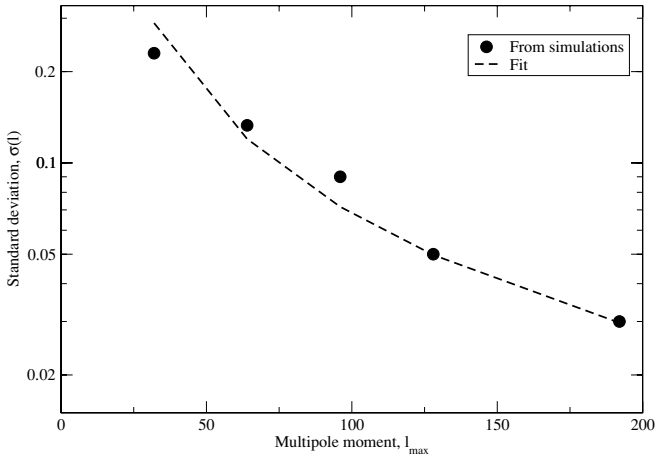

Figure 6. Estimated uncertainty in g_* as a function of ℓ (black dots) and a best-fit power-law function (red line) for cosmic variance limited data.

to a power law in ℓ, in good agreement with the arguments given by Pullen & Kamionkowski (2007) and Groeneboom & Eriksen (2009). The best-fit power-law function is

$$\sigma(\ell_{\rm high};\, g_*) = 0.0117 \left(\frac{\ell_{\rm high}}{400}\right)^{-1.27}, \qquad (12)$$

and this can be used to produce rough forecasts for the Planck experiment including polarization. For instance, if both temperature and E-mode polarization data are available up to $\ell = 512$, then the standard deviation of g_* is $\sigma(512) \sim 0.001$. This is generally a factor two better than using temperature alone.

7. CONCLUSIONS

We have generalized a previously developed Bayesian framework to allow for exact analysis of any general anisotropic universe models that predicts a sparse signal harmonic space covariance matrix, including polarization data. This generalization involved incorporation of a sparse matrix library into the existing Gibbs sampling code called "Commander." We implemented support for this model in our codes, before demonstrating and validating the new tools with appropriate simulations including polarization data. First, we compared the results from the Gibbs sampler with brute-force likelihood evaluations, and then verified that the input parameters were faithfully reproduced in realistic *WMAP* simulations.

We then considered a special case of anisotropic universe models, namely, the Ackerman et al. (2007) model which generalizes the primordial power spectrum $P(k)$ to include a dependence on direction, $P(\mathbf{k})$. The equations were however not complete, and the analysis performed by Groeneboom & Eriksen (2009) has been re-done including the previously neglected $(-i)^{l-l'}$-term.

We then analyzed the five-year *WMAP* temperature sky maps, and presented the updated *WMAP* posteriors of the ACW model. The results from this analysis are in accordance with the results from Hanson & Lewis (2009), showing that the preferred direction is now located at the ecliptic poles. This suggests that the signal is most likely not of cosmological origin, and its origin must be either from within the solar system or systematics.

We have investigated four cases of systematic effects that share similar structures with the ACW signal. We have shown that neither asymmetric beams, the zodiacal light, noise rms misestimation, nor possible pixel anti-correlations in the *WMAP* data could have given rise to the observed signal.

To summarize, we have shown that there exists a strong anisotropic signal corresponding to the ACW signal in all the *WMAP* data that is aligned with the north and south ecliptic poles. The probability that the axis should correspond so closely to the ecliptic poles is very low, indicating that the signal is due to a systematic effect. The signal makes up more than 5% of the total power of the temperature fluctuations in the CMB. We have excluded some of the possible candidates as source of the ACW signal. Determining the nature of the systematic effect will be of vital importance, as it might affect other cosmological conclusions from the *WMAP* experiment, and the upcoming Planck data will clearly be invaluable for understanding the nature of this feature.

We thank Liu Hao and Ti-Pei Li for supplying us with their one-year *WMAP* data. We acknowledge use of the HEALPix[7] software (Górski et al. 2005) and analysis package for deriving the results in this paper. We acknowledge the use of the Legacy Archive for Microwave Background Data Analysis (LAMBDA). Support for LAMBDA is provided by the NASA Office of Space Science. The authors acknowledge financial support from the Research Council of Norway.

APPENDIX

THE COVARIANCE MATRIX

Even though we do not employ B-mode polarization data in the analysis performed in this paper, the numerical framework still supports B-mode polarization. In this section, we therefore describe the full TT+EE+BB covariance matrix including correlations. In the previous analysis, only TT anisotropic correlations were considered. We now extend the framework to include polarization, such that the Fourier coefficients become

$$a_{\ell m} = \left(a_{\ell m}^{\rm TT}, a_{\ell m}^{\rm EE}, a_{\ell m}^{\rm BB}\right). \qquad (A1)$$

The covariance matrix $C_{\ell m,\ell' m'}$ can be expressed as

$$C_{\ell m,\ell' m'} = \begin{pmatrix} {\rm TT} & {\rm TE} & {\rm TB} \\ {\rm TE} & {\rm EE} & {\rm EB} \\ {\rm TB} & {\rm EB} & {\rm BB} \end{pmatrix}. \qquad (A2)$$

The existing framework for sampling anisotropic universe models in FORTRAN was then altered to allow for polarization data, and whether polarization is used is flagged through a parameter file. The off-diagonal TT+EE+BB anisotropic covariance matrix is presented in Figure 7. Note that the BB component is zero in this plot. However, this straightforward representation of the full covariance matrix is too naive: performing a Cholesky factorization (diagonalizing) of this matrix for high ℓs is nearly impossible. Diagonalizing a matrix is more efficient when off-diagonal elements are close to the diagonal. However, the (TT, EE, BB) representation of the matrix in Figure 7 gives rise to elements spread around the full matrix. Typically, Cholesky factorization for such a TT–EE–BB representation breaks down for $l_{\rm max} = 64$ due to the dense structure of the upper-triangular decomposed L-matrix.

To overcome this problem, we operate with a different representation of the (TT, EE, BB)-matrix. Instead of building

[7] http://healpix.jpl.nasa.gov

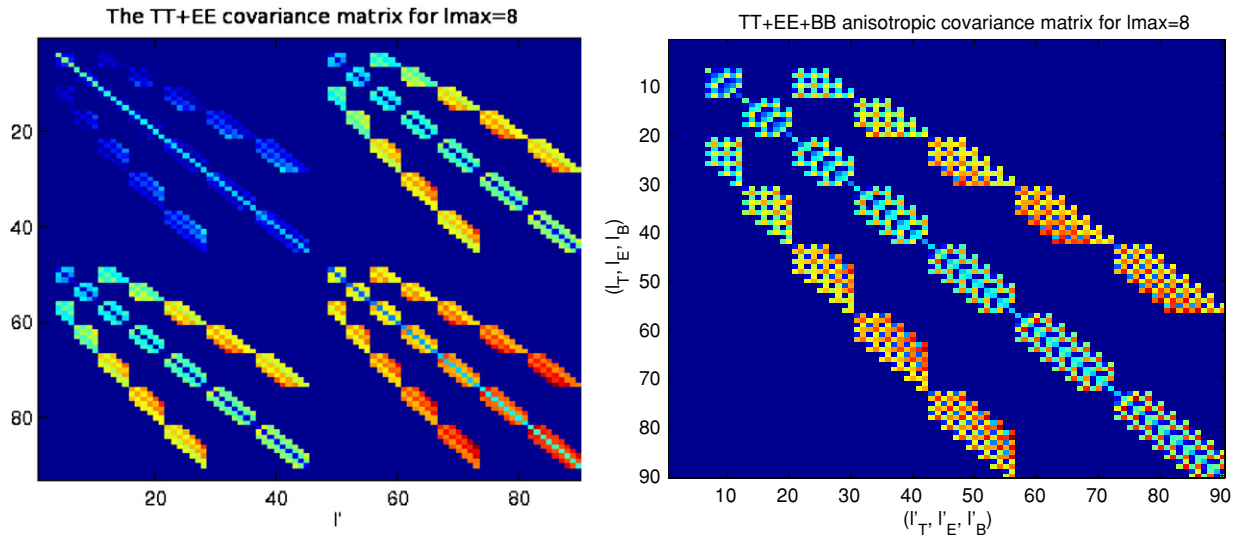

Figure 7. ACW TT–EE covariance matrix (left) in the representation of Equation (A2). Diagonalizing this matrix turns out to be a nearly impossible task, forcing us to use another representation. The ACW TT–EE covariance matrix (right) in the representation of Equation (A3). Diagonalizing this matrix is similar to diagonalizing the TT-only ACW covariance matrix and is more efficient.

(A color version of this figure is available in the online journal.)

the matrix as presented in Equation (A2), we choose a different way of expressing the matrix:

$$C_{\ell m,\ell' m'} = \begin{pmatrix} \mathrm{TT}_{00} & \mathrm{TE}_{00} & \mathrm{TB}_{00} & \mathrm{TT}_{10} & \dots & \mathrm{EE}_{n0} \\ \mathrm{TE}_{00} & \mathrm{EE}_{00} & \mathrm{EB}_{00} & \mathrm{TE}_{10} & \dots & \mathrm{EB}_{n0} \\ \mathrm{TB}_{00} & \mathrm{EB}_{00} & \mathrm{BB}_{00} & \mathrm{TB}_{10} & \dots & \mathrm{BB}_{n0} \\ \mathrm{TT}_{01} & \mathrm{TE}_{01} & \mathrm{TB}_{01} & \mathrm{TT}_{11} & \dots & \mathrm{EE}_{n1} \\ \vdots & \vdots & \vdots & \vdots & \dots & \vdots \\ \mathrm{TB}_{0n} & \mathrm{EB}_{0n} & \mathrm{BB}_{0n} & \mathrm{TB}_{1n} & \dots & \mathrm{BB}_{nn} \end{pmatrix} \tag{A3}$$

with corresponding $a_{\ell m}$s

$$a_{\ell m} = \left(a^T_{00}, a^E_{00}, a^B_{00}, a^T_{01}, \dots, a^B_{l_{\max},m(l_{\max})}\right). \tag{A4}$$

As the EE and BB correlations share the same structure as the stand-alone TT, the complete covariance matrix will in this representation resemble the original three-banded covariance matrix. The elements are now much closer to the diagonal, solving the problem of inefficient diagonalizing. The matrix representation is depicted in Figure 7. Note that this representation is only used when multiplying the matrices with vectors and performing Cholesky decompositions. Within the rest of the framework, the $a_{\ell m}$s are treated as in Equation (A1).

REFERENCES

Ackerman, L., Carroll, S. M., & Wise, M. B. 2007, Phys. Rev. D, 75, 083502
Bennett, C. L., et al. 2003, ApJS, 148, 1
Carroll, S. M., Tseng, C.-Y., & Wise, M. B. 2010, Phys. Rev. D, 81, 083501
de Oliveira-Costa, A., Tegmark, M., Zaldarriaga, M., & Hamilton, A. 2004, Phys. Rev. D, 69, 063516
Dimopoulos, K., Karčiauskas, M., Lyth, D. H., & Rodríguez, Y. 2009, J. Cosmol. Astropart. Phys., JCAP05(2009)013
Dvorkin, C., Peiris, H. V., & Hu, W. 2008, Phys. Rev. D, 77, 063008
Eriksen, H. K., Dickinson, C., Jewell, J. B., Banday, A. J., Górski, K. M., & Lawrence, C. R. 2008a, ApJ, 672, L87
Eriksen, H. K., Hansen, F. K., Banday, A. J., Górski, K. M., & Lilje, P. B. 2004a, ApJ, 609, 1198
Eriksen, H. K., Huey, G., Banday, A. J., Górski, K. M., Jewell, J. B., O'Dwyer, I. J., & Wandelt, B. D. 2007a, ApJ, 665, L1
Eriksen, H. K., Jewell, J. B., Dickinson, C., Banday, A. J., Górski, K. M., & Lawrence, C. R. 2008b, ApJ, 676, 10
Eriksen, H. K., et al. 2004b, ApJS, 155, 227
Eriksen, H. K., et al. 2007b, ApJ, 656, 641
Gold, B., et al. 2009, ApJS, 180, 265
Górski, K. M., Hivon, E., Banday, A. J., Wandelt, B. D., Hansen, F. K., Reinecke, M., & Bartelmann, M. 2005, ApJ, 622, 759
Groeneboom, N. E. 2009, arXiv:0905.3823
Groeneboom, N. E., & Eriksen, H. K. 2009, ApJ, 690, 1807
Groeneboom, N. E., Eriksen, H. K., Gorski, K., Huey, G., Jewell, J., & Wandelt, B. 2009, ApJ, 702, L87
Guth, A. H. 1981, Phys. Rev. D, 347
Hanson, D., & Lewis, A. 2009, arXiv:0908.0963
Himmetoglu, B., Contaldi, C. R., & Peloso, M. 2009a, Phys. Rev. D, 79, 063517
Himmetoglu, B., Contaldi, C. R., & Peloso, M. 2009b, Phys. Rev. D, 102, 111301
Hinshaw, G., et al. 2007, ApJS, 170, 288
Hinshaw, G., et al. 2009, ApJS, 180, 225
Hou, Z., Banday, A. J., Gorski, K. M., Groeneboom, N. E., & Eriksen, H. K. 2009, arXiv:0910.3445
Jewell, J., Levin, S., & Anderson, C. H. 2004, ApJ, 609, 1
Karčiauskas, M., Dimopoulos, K., & Lyth, D. H. 2009, Phys. Rev. D, 80, 023509
Kelsall, T., et al. 1998, ApJ, 508, 44
Komatsu, E., et al. 2009, ApJS, 180, 330
Larson, D. L., Eriksen, H. K., Wandelt, B. D., Górski, K. M., Huey, G., Jewell, J. B., & O'Dwyer, I. J. 2007, ApJ, 656, 653
Limon, M., et al. 2008, The Wilkinson Microwave Anisotropy Probe (WMAP) Experiment, The Five-Year Explanatory Supplement (Greenbelt, MD: NASA/GSFC)
Linde, A. D. 1982, Phys. Lett. B, 108, 389
Linde, A. D. 1983, Phys. Lett. B, 155, 295
Linde, A. D. 1994, Phys. Rev. D, 49, 748
Liu, H., & Li, T.-P. 2009a, arXiv:0907.2731
Liu, H., & Li, T. 2009b, Sci. China G: Phys. Astron., 52, 804
Mukhanov, V. F., & Chibisov, G. V. 1981, ZhETF Pisma Redaktsiiu, 33, 549
O'Dwyer, I. J., et al. 2004, ApJ, 617, L99
Pullen, A. R., & Kamionkowski, M. 2007, Phys. Rev. D, 76, 103529
Ruhl, J. E. 2003, ApJ, 599, 786
Runyan, M. C. 2003, ApJS, 149, 265
Scott, P. F., et al. 2003, MNRAS, 341, 1076
Smoot, G. F. 1992, ApJ, 396, L1
Spergel, D. N., et al. 2007, ApJS, 170, 377
Starobinsky, A. A. 1982, Phys. Lett. B, 117, 175
The Planck Collaboration 2006, arXiv:astro-ph/0604069
Valenzuela-Toledo, C. A., & Rodriguez, Y. 2009, arXiv:0910.4208
Valenzuela-Toledo, C. A., Rodriguez, Y., & Lyth, D. H. 2009, arXiv:0909.4064
Vielva, P., Martínez-González, E., Barreiro, R. B., Sanz, J. L., & Cayón, L. 2004, ApJ, 609, 22
Wandelt, B. D., Larson, D. L., & Lakshminarayanan, A. 2004, Phys. Rev. D, 70, 8
Wehus, I. K., Ackerman, L., Eriksen, H. K., & Groeneboom, N. E. 2009, ApJ, in press (arXiv:0904.3998)